

A Theoretical Comparison of Lewis Acid vs Bronsted Acid Catalysis for *n*-Hexane → Propane + Propene

Qingbin Li, Ken C. Hunter,[†] and Allan L. L. East*

Department of Chemistry and Biochemistry, University of Regina, Regina, Saskatchewan, S4S 0A2, Canada

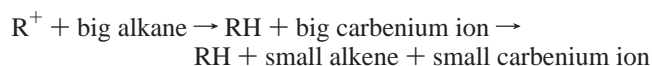
Received: January 12, 2005; In Final Form: May 21, 2005

Cracking of an all-trans *n*-alkane, via idealized Lewis acid and Bronsted acid catalysis, was examined using density functional theory. Optimized geometries and transition states were determined for catalyst–reactant complexes, using AlCl₃ and HCl·AlCl₃ as the Lewis and Bronsted acids. For the Lewis acid cycle, hydride-transfer steps are seen to have large barriers in both forward and reverse directions, and an unstable physisorbed carbenium ion (lying 20 kcal mol⁻¹ above the chemisorbed intermediate) is the launching point for the β-scission that leads to products. For the Bronsted acid cycle, proton-transfer steps have smaller barriers in both forward and reverse directions, and a semistable physisorbed alkanium ion is the launching point for the alkanium α-scission that leads to products. In the idealized Lewis cycle, formation of HCl units (and hence Bronsted acids) was found to be a common side reaction. A recent ionic-liquid catalysis study is mentioned as motivation, although our study is not a computational modeling study; we are more interested in the fundamental differences between Bronsted and Lewis mechanisms rather than merely mimicking a particular system. However, results of exploratory optimizations of various intermediates with Al₂Cl₇⁻ as the catalyst are presented to provide the first step for future modeling studies on the ionic liquid system.

Introduction

Room-temperature ionic liquids (RTILs) have recently been gaining popularity as “green chemistry” solvents in organic synthesis, because they are nonvolatile, have low energy requirements, can dissolve a range of reactants and catalysts, and can provide ease of product extraction.^{1–3} In many cases, often involving chloroaluminate-based RTILs, these liquids themselves serve as the catalysts, for reactions such as ether cleavage,^{4,5} Friedel–Crafts alkylation of benzene,⁶ oligomerization of alkenes,⁷ and polyethylene cracking.⁸ Of particular interest to us is the recent report of Xiao et al. of both Bronsted acid and Lewis acid catalysis of alkane cracking in the ionic liquid C₅H₅NH⁺·Al₂Cl₇⁻.⁹

Solid zeolites, and liquid superacids¹⁰ such as HF·SbF₅ and HSO₃F·SbF₅ (having a great deal of ionic-liquid character), are capable of cracking alkanes. The cracking is generally performed by carbenium ions in a chain reaction,¹¹ e.g.



The initiation steps that generate carbenium ions R⁺ are either redox or Bronsted attack of an alkane or Bronsted attack of trace amounts of alkene.

Seventy years ago, pure AlCl₃ (Al₂Cl₆) was shown to be incapable of cracking alkanes but became capable upon exposure to chloroalkane or Bronsted acid impurities.¹² The initiation steps of these “active” forms of AlCl₃ can be understood in the following ways: (i) AlCl₃ can abstract chloride from a chloroalkane, creating a carbenium ion, or (ii) AlCl₃ can enhance

the Bronsted acidity of a Bronsted acid impurity by promoting proton loss, achieving a Bronsted initiation step on a hydrocarbon to create a carbenium ion. On the other hand, pure aluminum chloride evidently cannot perform Lewis-acid hydride-abstraction on an alkane as an initiation step. Today, Lewis-acid hydride abstraction is rarely discussed as a C–H-bond activation step; a review by Corna and Garcia¹³ of general Lewis acid catalysis does not address alkane cracking, and a review by Fokin and Schreiner¹⁴ of C–H-bond functionalization prefers to talk of radical intermediates or “hydrogen-coupled electron transfer” when discussing electrophilic attack of alkanes. Hence, the claim of Xiao et al.⁹ of a Lewis acid mechanism is quite intriguing. Unfortunately, it is *far too premature* to attempt a computational modeling study of a possible Lewis acid mechanism by ionic liquid catalysts, because an ionic liquid is very complex, and we found no prior knowledge of a chloroaluminate-catalyzed reaction path for *any* reaction.

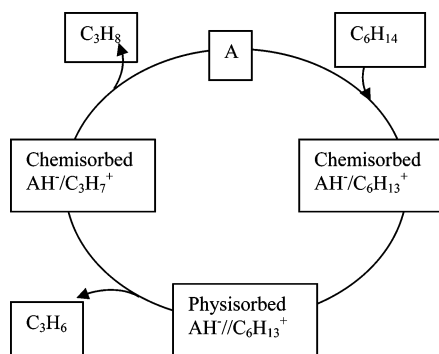
In this journal in 2003, our group published a theoretical study on an idealized Bronsted acid catalytic cycle for hexane → propane + propene.¹⁵ There we demonstrated that, when other real-system effects are removed, the existence of certain intermediates can still vary with catalyst, simply due to acidity of the catalyst. Here we wish to present a sister paper, looking at the same reaction but with a Lewis acid catalyst, to contrast the Lewis and Bronsted mechanisms for the same reaction. However, since the previous study began with cationic catalysts and no extra charge separation in the activation step and here we wished to perform a Lewis cycle with neutral AlCl₃ and charge separation in the activation step, we have added a new Bronsted acid cycle here, with neutral HCl·AlCl₃ as the catalyst.

This paper is a computational study of the minimum-energy pathways used by a single Lewis acid molecule AlCl₃ or a single Bronsted acid molecule HCl·AlCl₃ in performing a complete catalytic cycle for the reaction *n*-hexane → propane + propene.

* To whom correspondence may be addressed. E-mail: allan.east@uregina.ca.

[†] Present address: Department of Chemistry, Mount Allison University, Sackville, NB E4L 1E4 Canada.

SCHEME 1: Hypothetical Four-Step Lewis Acid Catalytic Cycle for Hexane \rightarrow Propane + Propene, via Lewis Acid A



In addition, we have included some exploratory calculations of possible intermediates (minima) if Al_2Cl_7^- were chosen as the Lewis acid model, to infer how relevant this idealized AlCl_3 mechanism might be to the system of Xiao et al.⁹ Contrast between Bronsted acid and Lewis acid mechanisms is the focus of this work; we are avoiding computational modeling because this would bring in extra effects (and approximations) that would prevent us from properly performing the ideal comparison.

Scheme 1 shows the hypothetical Lewis acid catalytic cycle considered for exploratory investigation. Note that we distinguish between chemisorbed and physisorbed complexes, with single and double slashes (/ and //), respectively; see Methods section for more description. After physisorption of free hexane onto the Lewis acid catalyst A, making $\text{C}_6\text{H}_{14}//\text{A}$, the first step is *hydride extraction* from the second carbon of hexane by A, likely generating a chemisorbed $\text{C}_6\text{H}_{13}^+/\text{AH}^-$ complex. In the second step we imagine an *ascension* from a chemisorbed to a physisorbed $\text{C}_6\text{H}_{13}^+//\text{AH}^-$ state. This physisorbed ion-pair state may or may not require an isomerization in order to proceed. If not, then the third step would be the β -*scission* of $\text{C}_6\text{H}_{13}^+$ to form a likely chemisorbed $\text{C}_3\text{H}_7^+/\text{AH}^-$ complex with an evolved or physisorbed C_3H_6 . In the fourth step, we imagine a *hydride back-transfer* from the catalyst to the ascending C_3H_7^+ unit to form an evolved or physisorbed propane molecule. The reader will see that the exploration of this hypothesis led to other steps that needed to be considered.

Theoretical Methods

All calculations used the common semiempirical density functional theory (DFT) model B3LYP,^{16,17} with the 6-31G-(d,p) basis set.¹⁸ The Gaussian98 code¹⁸ was predominantly used for minimizations. The PQS 3.0 code¹⁹ was used for transition-state searches because of its parallelism and because the Baker eigenvector following algorithm²⁰ is not restricted to 50 variables, as it is in Gaussian98. However, because the default grid in PQS 3.0 is finer, the B3LYP energies between the two codes are not compatible, and final results were run with Gaussian98. Molecular geometries and harmonic frequencies were computed using analytic first and second derivative formulas as is routine with most quantum chemistry codes. The energies reported are not obscured by thermal contributions but are corrected for zero-point vibrational energies (ZPVE) using the usual $3N - 6$ or $3N - 7$ harmonic contributions for minima and transition states, respectively.

Explicit contact modeling was used with small fragment model of catalysts to compute real transition states in full-coordinate space and to carefully follow the connections from these to the intermediates that they connect. For most stationary

TABLE 1: Computed Desorption Energies (B3LYP/6-31G(d,p) with ZPVE, kcal mol⁻¹)

desorption	ΔE
$\text{C}_6\text{H}_{12}/\text{HCl}/\text{AlHCl}_2 \rightarrow \text{C}_6\text{H}_{12}/\text{HCl} + \text{AlHCl}_2$	11.4
$\text{C}_6\text{H}_{12}/\text{HCl}/\text{AlHCl}_2 \rightarrow \text{C}_6\text{H}_{12} + \text{HCl}/\text{AlHCl}_2$	9.4
$\text{HCl}/\text{AlHCl}_2 \rightarrow \text{HCl} + \text{AlHCl}_2$	4.9
$\text{C}_6\text{H}_{12}/\text{HCl} \rightarrow \text{C}_6\text{H}_{12} + \text{HCl}$	2.9
$\text{C}_3\text{H}_6/\text{C}_3\text{H}_6/\text{HCl}/\text{AlHCl}_2 \rightarrow \text{C}_3\text{H}_6 + \text{C}_3\text{H}_6/\text{HCl}/\text{AlHCl}_2$	2.3
$\text{C}_3\text{H}_6/\text{C}_3\text{H}_7^+/\text{AlHCl}_3^- \rightarrow \text{C}_3\text{H}_6 + \text{C}_3\text{H}_7^+/\text{AlHCl}_3^-$	2.1
$\text{C}_6\text{H}_{14}/\text{AlCl}_3 \rightarrow \text{C}_6\text{H}_{14} + \text{AlCl}_3$	1.5
$\text{C}_3\text{H}_6/\text{C}_3\text{H}_8/\text{AlCl}_3 \rightarrow \text{C}_3\text{H}_6 + \text{C}_3\text{H}_8/\text{AlCl}_3$	0.6

points, there is more than one possible orientation of the reactant relative to the catalyst, and a few possibilities were investigated, although these possibilities are usually indistinguishable in energy on the scale of the reaction pathway. Our atom-numbering convention will be to count the carbon atoms as C₁, C₂, C₃, C₄, C₅, and C₆ such that the C₂ atom is the one which loses the hydride to the catalyst in the first step and becomes only bound to the Cl₁ atom of the catalyst in the chemisorbed state.

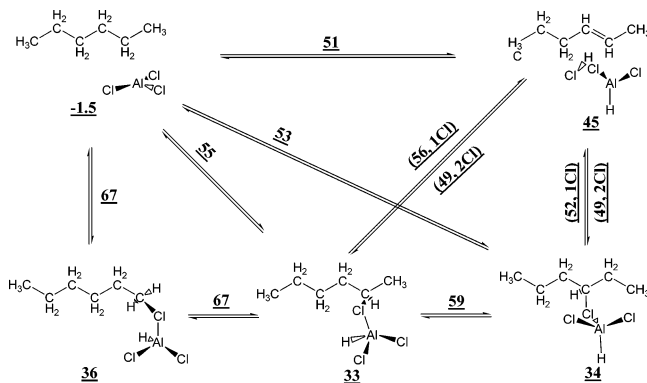
The transition states that were located had only one imaginary vibrational frequency corresponding to the desired reaction coordinate. Each transition state was validated by two verification minimizations (to locate the two relevant intermediates) from displaced geometries on either side of the transition state. The displaced geometries for these verification runs were obtained by identifying the key internal coordinates in the crucial normal mode via the animation of the imaginary frequency and then displacing these coordinates in both directions (minus or plus 0.03 Å for bond lengths; minus or plus 3° for angles and dihedrals).

We will use the word physisorbed to describe van der Waals neutral-pair complexes of catalyst and reactant, but also ion-pair (cation–anion, or sometimes called “zwitterionic”) complexes. Although ion-pair complexes are sometimes thought to have an ionic bond strong enough to be considered chemisorbed, in our systems the dissociation energies are much smaller because a proton transfer would occur if the molecular ions were pulled apart, resulting in neutral dissociated molecules. Although the concepts of chemisorbed and physisorbed states are taken from surface-science terminology,²¹ we think these states may prove to be pervasive in homogeneous as well as heterogeneous catalysis. We will use single and double slashes to denote chemisorbed and physisorbed complexes, respectively (e.g., $\text{C}_6\text{H}_{13}^+/\text{AlHCl}_3^-$ vs $\text{C}_6\text{H}_{13}^+//\text{AlHCl}_3^-$). We will refer to the conversion from chemisorbed to physisorbed as ascension and the opposite as descension, since the terms desorption and adsorption strictly refer to molecules leaving and approaching the surface.²²

Finally, we define some abbreviations for the rest of the article: PES, potential energy surface; CP, dialkylcyclopropane; PCP⁺, protonated dialkylcyclopropane²³ (the prevalent form of a poorly solvated or gas-phase secondary carbenium ion).

Results

Desorption Energies of Physisorbed Complexes. Several minimized complexes, particularly ones involving AlCl_3 , are difficult to classify as either physisorbed or chemisorbed from geometric structures alone. Table 1 lists several computed desorption energies to justify the use of the term “physisorbed” for many such cases. Note the inherent synergistic three-body stability of the triple complex $\text{C}_6\text{H}_{12}/\text{HCl}/\text{AlCl}_3$: it requires 9–11 kcal mol⁻¹ to desorb the first fragment and 3–5 kcal mol⁻¹ to desorb the second fragment, *regardless* of whether C_6H_{12} or AlCl_3 is desorbed first. We suggest that the low binding

SCHEME 2: Overview of B3LYP/6-31G(d,p) Results for the First Part of the Lewis Acid Catalytic Cycle^a


^a Various hydride abstractions from hexane (top left), plus isomerization among the various intermediates. The bottom row has various chemisorbed hexenium ions, while the top right has the physisorbed 2-hexene intermediate. Underlined numbers indicate ZPVE-corrected energies of minima and transition states (kcal mol⁻¹) relative to uncomplexed hexane + AlCl₃.

energies in the table warrant use of the term “physisorbed” to describe their interactions. In contrast, we will refer to a “chemisorbed” hexenium ion complex, because C₆H₁₃⁺/AlHCl₃⁻ → C₆H₁₂ + HCl//AlCl₃ has a computed Δ*E* of 22 kcal mol⁻¹. This chemisorbed complex is analogous to the alkoxy structures²⁴ (surface-bound carbenium ions¹¹) in zeolite-catalyzed hydrocarbon modification.

Catalysis by AlCl₃. In this section we describe, in order, the individual steps in the Lewis acid catalytic cycle.

Scheme 2 shows an overview of our results for the initial hydride-abstraction step and ensuing isomerization possibilities. We found transition states for hydride abstractions leading to 4 unique products: 3 to chemisorbed hexenium complexes (1-hexenium, 2-hexenium, 3-hexenium) and 1 to physisorbed hexene. The formation of 1-hexenium ion has the highest reaction barrier (68.5 kcal mol⁻¹), which is not a surprise. The other three activation energies are also high (52–57 kcal mol⁻¹), with the formation of physisorbed hexene//HCl//AlCl₃ slightly kinetically favored over the formation of chemisorbed secondary hexenium ions; however, these chemisorbed hexenium ions are substantially thermodynamically favored over the physisorbed hexene complex.

Figure 1 shows the 3D images of the stationary-point geometries for the 4 different versions of hydride abstraction. All reaction paths start with the aluminum atom in the catalyst coordinated to an accessible hydrogen on the secondary or primary carbon. The four transition states all have a great deal of ion-pair character. In the top row, a hydride (from C2 to Al) and a proton (from C3 to Cl1) both transfer from hexane to the catalyst, with the transition state featuring the hydride transfer completed and the proton transfer in progress. The product features a newly formed HCl unit, with its Cl coordinated to the AlHCl₂ and its H coordinated to the double bond of hexene. In the other three rows, the hydride extraction results in an ion-pair transition state, which then descends to a Cl-bridged chemisorbed hexenium-ion complex.

Scheme 2 also shows isomerization between chemisorbed forms of hexenium ion, which have large barriers of 25 kcal mol⁻¹ or larger. However, the barriers to form the higher-energy physisorbed 2-hexene complex are smaller. This physisorbed hexene complex at 45 kcal mol⁻¹ only requires 3–4 kcal mol⁻¹ more energy to descend back to a chemisorbed hexenium state.

Hydride abstraction from hexane		
M1	TS	M2
 -1860.146621	 -1860.062856	 -1860.071154
 -1860.146066	 -1860.036849	 -1860.085150
 -1860.146443	 -1860.056484	 -1860.091360
 -1860.145542	 -1860.058879	 -1860.090132

Figure 1. B3LYP/6-31G(d,p) stationary points for four different hydride abstraction steps. Molecular energies in au include ZPVE. Top row: forming physisorbed 2-hexene. Next three rows: forming chemisorbed 1-hexenium, 2-hexenium, and 3-hexenium ions, respectively.

Figure 2 shows the 3D images of stationary points for six different isomerization paths. The top two rows are isomerizations between chemisorbed hexenium ions; note that the chlorine atom bridge between reactant and catalyst jumps from carbon to neighboring carbon underneath the molecule, while a hydride ion does the same shift in the opposite direction above the molecule. Also note that in the transition state the carbon atoms changed hybridization from sp³ to sp² before returning to sp³. The lower four rows in Figure 2 show ascensions from chemisorbed C₆H₁₃⁺/AlHCl₃⁻ to physisorbed hexene//HCl//AlHCl₂; note that these transition states are late and occur during the final H⁺ transfer to the catalyst, after the C–Cl bond has dissociated. The third and fifth rows are called “one-chlorine paths” because the chlorine that accepts the proton transfer is Cl1, the one that was bonded to the carbenium ion center. In the fourth and sixth rows, a different chlorine (Cl2) is the one accepting the proton.

The top half of Scheme 3 shows the overview of our results for the entire Lewis cycle, ignoring some of the isomerizations of Scheme 2. In this scheme, the horizontal coordinate is a crude coordinate representing the general stepwise reaction path of hydride abstraction, ascension, β-scission, and hydride back-transfer, while the vertical coordinate represents the ion-pair vs neutral-pair state of the physisorbed complexes (ion pair on the bottom, neutral pair on the top). We next discuss the steps leading from the chemisorbed hexenium ion complex at 33 kcal mol⁻¹.

The ascension of chemisorbed hexenium ions to physisorbed PCP⁺ ions is next, and the top two rows of Figure 3 show the 3D images of stationary points for two such ascensions. The transition states are very late, with the CCC ring-closing almost complete. The PCP⁺ ion (right-hand column) has an edge-protonated cyclopropane ring, where the three carbons and the extra H⁺ lie nearly planar, and the C2C3C4 angle is around

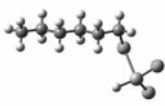
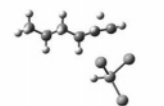
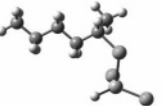
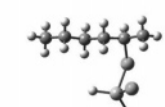
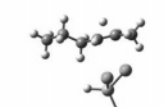
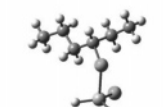
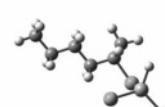
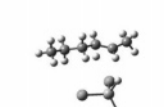
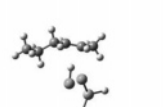
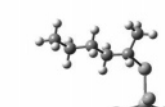
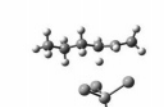
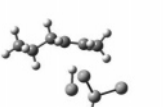
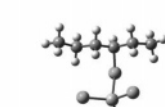
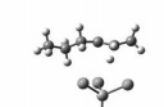
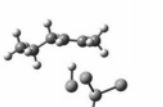
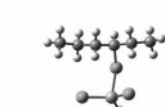
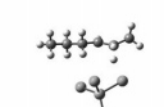
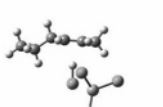
Isomerization of chemisorbed hexenium ions		
M1	TS	M2
 -1860.086331	 -1860.037429	 -1860.089275
 -1860.090205	 -1860.050124	 -1860.088980
Ascension to physisorbed hexene		
M1	TS	M2
 -1860.090676	 -1860.054888	 -1860.071175
 -1860.092041	 -1860.066547	 -1860.072499
 -1860.090454	 -1860.061695	 -1860.072500
 -1860.090399	 -1860.065781	 -1860.072499

Figure 2. B3LYP/6-31G(d,p) stationary points for six different isomerization paths. Top two rows: 1-hexenium to 2-hexenium and 2-hexenium to 3-hexenium, respectively. Next two rows: ascension of chemisorbed 2-hexenium ion to physisorbed 2-hexene via the “one-chlorine” and “two-chlorine” paths, respectively. Last two rows: ascension of chemisorbed 3-hexenium ion to physisorbed 2-hexene via the “one-chlorine” and “two-chlorine” paths, respectively.

80°. Neither PCP⁺ image indicates a completely closed CCC ring because the C2–C4 bond is rather long (2.0 Å).

With great effort, we found two ion-pair and two neutral-pair physisorbed-complex intermediates and transition states for proton transfers between the ion-pair and neutral-pair forms. We found a proton transfer from a precarious physisorbed 2-hexenium ion to catalyst, making hexene; however, the barrier to transfer was so tiny that it was lost upon ZPVE correction, and hence we chose not to report the data. We also found a proton transfer from PCP⁺ to catalyst, making CP, and this does appear in Scheme 3 and Figure 3. Proton-transfer appears to be somewhat facile when the system is in the physisorbed state.

Direct β -scission of hexenium ion from a chemisorbed state is not a minimum-energy pathway on the B3LYP/6-31G(d,p) PES. Only a precarious ion-pair PCP⁺//AlHCl₃⁻ complex was found to undergo the cracking step. Figure 4 displays the 3D images of the relevant stationary points. In the first two rows of Figure 4, the scission of cis- and trans-PCP⁺ ion-pair

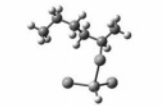
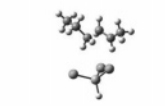
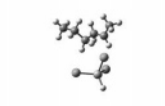
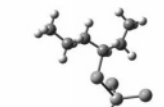
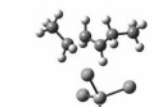
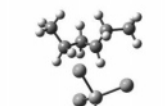
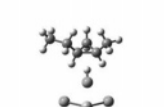
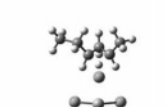
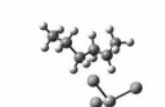
Ascension to physisorbed PCP cation		
M1	TS	M2
 -1860.089832	 -1860.055039	 -1860.055671
 -1860.091384	 -1860.056333	 -1860.056858
Neutral-pair to ion-pair conversion		
M1	TS	M2
 -1860.051263	 -1860.050191	 -1860.056819

Figure 3. B3LYP/6-31G(d,p) stationary points for steps which generate physisorbed ion-pair complexes. Top two rows: ascension of 2-hexenium and 3-hexenium ions, respectively, to PCP⁺//AlHCl₃⁻. Third row: proton transfer converting CP to PCP⁺.

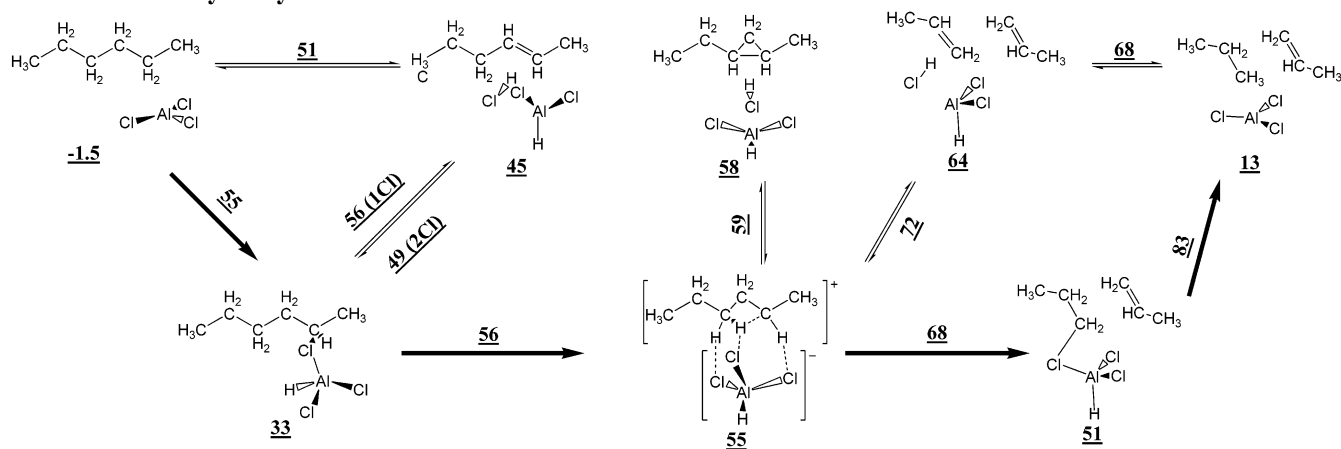
complexes to chemisorbed propenium ions and propene are shown (bold-arrow route 55–68–51 in Scheme 3). The transition states feature an S_N2-type substitution for this step, with the C4 atom accepting a chlorine bridge and expunging the C3 and C2 atoms of the protonated cyclopropane ring, resulting in cleavage of the original C4–C3 bond. In the bottom row of Figure 4, a never-before-seen version of the scission step is presented, in which physisorbed PCP⁺ dissociates into a physisorbed complex of two propene molecules. In the transition state, the C4–C3 bond is essentially broken (2.9 Å), and the final proton transfer to the catalyst is just beginning. This scission has a barrier of 17 kcal mol⁻¹, which is significantly higher than the 13 kcal mol⁻¹ barrier leading to chemisorbed propenium ion; however, it leads to a lower-energy pathway for completing the catalytic cycle (see Scheme 3). The reverse of this step is also interesting, because it implies that Bronsted-acid-catalyzed oligomerization of alkenes does not necessarily have to go through a chemisorbed state.

After the scission step, we removed the produced propene (assumed to have left the complex), and tackled the hydride back-transfer step to regenerate the AlCl₃ catalyst. This was the conversion of C₃H₇⁺/AlHCl₃⁻ or C₂H₆/HCl//AlHCl₂ into C₃H₈//AlCl₃. Images of the optimized structures and transition state appear in Figure 5. In the top-row path of Figure 5, the transition state from chemisorbed primary propenium ion occurs after a partial ascension and features the approaching hydride and departing chloride at roughly equal distances from the C4 carbenium center. In the bottom-row path, both H⁺ and H⁻ transfer from the catalyst; the transition state occurs after the proton transfer to C4 but before the hydride transfer to C5 has begun. In both cases, the result is a final, tight physisorbed complex of propane with AlCl₃.

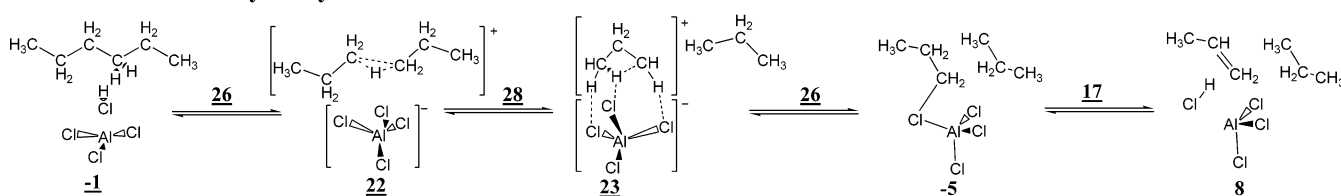
Catalysis by HCl•AlCl₃. The bottom half of Scheme 3 shows the overview of our results for the entire Bronsted cycle. In the first step, the HCl•AlCl₃ catalyst transfers the Bronsted proton to the central C–C bond of hexane, generating a physisorbed hexenium ion with a CHC three-center-two-electron bond. In the second step, the hexenium ion dissociates to produce propane

SCHEME 3: Overview of B3LYP/6-31G(d,p) Results for the Overall Cycles^a

Lewis-acid Catalysis Cycle



Bronsted-acid Catalysis Cycle



^a The Lewis acid cycle results ignore the 1-hexenium and 3-hexenium routes of Scheme 2, and the bold arrows indicate the path originally hypothesized in Scheme 1. Chemisorbed structures are drawn with covalent bonds between hydrocarbon and catalyst. Underlined numbers indicate ZPVE-corrected energies of minima and transition states (kcal mol⁻¹) relative to uncomplexed hexane + catalyst.

β-scission		
M1	TS	M2
 -1860.055672	 -1860.035955	 -1860.062342
 -1860.057188	 -1860.035737	 -1860.062179
 -1860.056820	 -1860.029956	 -1860.041565

Figure 4. B3LYP/6-31G(d,p) stationary points for three different β -scission (cracking) reactions. Top two rows: scission of *cis*-PCP⁺ and *trans*-PCP⁺, respectively, both forming chemisorbed propenium ion and propene. Bottom row: scission of *cis*-PCP⁺ to directly form two physisorbed propenes.

and physisorbed protonated cyclopropane. In the third step, this physisorbed protonated cyclopropane descends to a lower-energy chemisorbed propenium state. In the fourth step, the propenium ion re-ascends but transfers a proton back to the catalyst, regenerating the catalyst and producing physisorbed propene.

Figure 6 shows the 3D images of the stationary points for these four steps. In the C₆H₁₄/HCl/AlCl₃ complex, the H-Cl bond is aimed at a C-H bond density on the hexane, but due to the absence of a C-H-protonated hexanum ion isomer minimum, the transition state lies further along, with the proton nearly

Hydride back-transfer (catalyst regeneration)		
M1	TS	M2
 -1742.222047	 -1742.171926	 -1742.281952
 -1742.201217	 -1742.195299	 -1742.282851

Figure 5. B3LYP/6-31G(d,p) stationary points for the hydride back-transfer step to regenerate catalyst. Top row: ascension of propenium ion with hydride back-transfer. Bottom row: one-step conversion of propene to propane via proton and hydride transfer from catalyst.

fully transferred to a C-C bond. In the second step, hexanum ion dissociation produces C₃H₈/C₃H₇⁺//AlCl₄⁻, with the C₃H₇⁺ propenium ion in a PCP⁺ form. In the third step, PCP⁺ rotates to allow a nucleophilic chloride atom to chemisorb to a carbon atom, thereby expanding the CCC bond angle. In the fourth step, atom C4 leaves a chloride atom while a proton from C5 transfers to a different chloride (a 2Cl pathway).

This Bronsted path should be compared to our previous Bronsted-path analysis for this reaction.¹⁵ First, the first step goes directly to a C-C-protonated hexanum ion rather than an initial C-H-protonated isomer, because the catalyst's conjugate base is not weak enough to leave a stable C-H-protonated structure; in this respect the path is similar to the ones where H₃O⁺ or NH₄⁺ were the Bronsted acids. Second, physisorbed hexanum ion and ensuing physisorbed PCP⁺ are intermediates, as they were in all cases we studied previously.

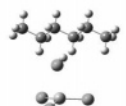
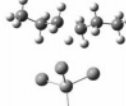
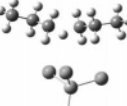
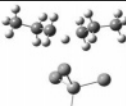
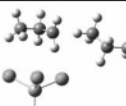
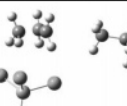
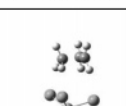
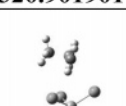
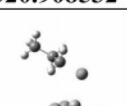
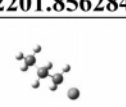
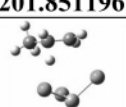
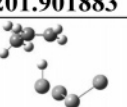
Bronsted-acid catalysis cycle		
M1	TS	M2
 -2320.947529	 -2320.903833	 -2320.910241
 -2320.910291	 -2320.901901	 -2320.908532
 -2201.856284	 -2201.851196	 -2201.901883
 -2201.901885	 -2201.866282	 -2201.880975

Figure 6. B3LYP/6-31G(d,p) stationary points for Bronsted acid catalysis cycle. Top row: protonation of C–C bond to form hexanium ion. Second row: α -scission of hexanium ion. Third row: descension of PCP⁺ to chemisorbed propenium ion. Bottom row: ascension of propene with proton back transfer to regenerate catalyst.

Third, and most dramatically, the PCP⁺-to-propene steps are very different here than in the previous project; here PCP⁺ descends to chemisorbed propenium ion before ascending to physisorbed propene, while the previous project showed PCP⁺ isomerizing to *physisorbed secondary propenium ion* before forming propene via proton-back-transfer to catalyst. The reason for the difference is that the catalyst here offers three nucleophilic atoms to the reagent (only one in the previous study) and hence greater ease for both the chemisorption of propenium and the ascension of propene. We did find a transition state for

a chemisorbed *p*-C₃H₇⁺ to chemisorbed *s*-C₃H₇⁺ isomerization, followed by ascension and proton transfer to create physisorbed propene, but the barriers were higher than those of the current path. This gives further evidence that primary carbenium ions need not convert to secondary carbenium ions when formed in solution.

Energy Profiles of the Bronsted and Lewis Catalytic Cycles. The energies for the overall catalytic cycles are plotted in Figures 7 (Lewis) and 8 (Bronsted). The energies are taken from Scheme 3 but for one minor detail. In Figure 7, near $x = 3.5$, there is a small 1–3 kcal mol⁻¹ rise after the scission steps due to the desorption of propene from the complex before continuing. In Scheme 3, however, this produced propene is assumed to remain physisorbed to the rest of the complex, so there the remaining Lewis cycle stationary-point energies have been lowered by 2 kcal mol⁻¹ to account for the extra adsorption energy. In both Figures 7 and 8, the overall energy profile is begun and completed with uncomplexed reactants and products, so that the overall $\Delta E = 17$ kcal mol⁻¹ is for the title reaction C₆H₁₄ → C₃H₈ + C₃H₆ independent of catalyst.

In the Lewis acid cycle (Figure 7), the overall reaction barrier occurs at the catalyst-regeneration step. The tenuous stability of the physisorbed ion-pair complex ($x = 2.5$) is very apparent. The dashed lines in Figure 7 show that, for this idealized system, lower barriers for both hydride-transfer steps are possible by passage through neutral-pair, Bronsted-acid-type complexes.

True Lewis-acid ionic liquids will have a PES that differs from Figure 7 in some important ways. First, ion-pair intermediates and transition states will be preferentially lowered (stabilized) vis-à-vis the neutral-pair Bronsted-acid-type ones, likely making the latter less relevant. Second, hydride-transfer steps will likely involve two solvent molecules and true S_N2 substitution with inversion at the carbon center, which will further lower these barriers.

In the Bronsted acid cycle (Figure 8), the overall reaction barrier occurs at the hexanium dissociation step. The chemisorbed intermediate C₃H₈/C₃H₇⁺/AlCl₄⁻ is a dramatic dip in the profile and is the lowest point on the reaction PES. The large (9 kcal mol⁻¹) decomplexation energy at the end of the

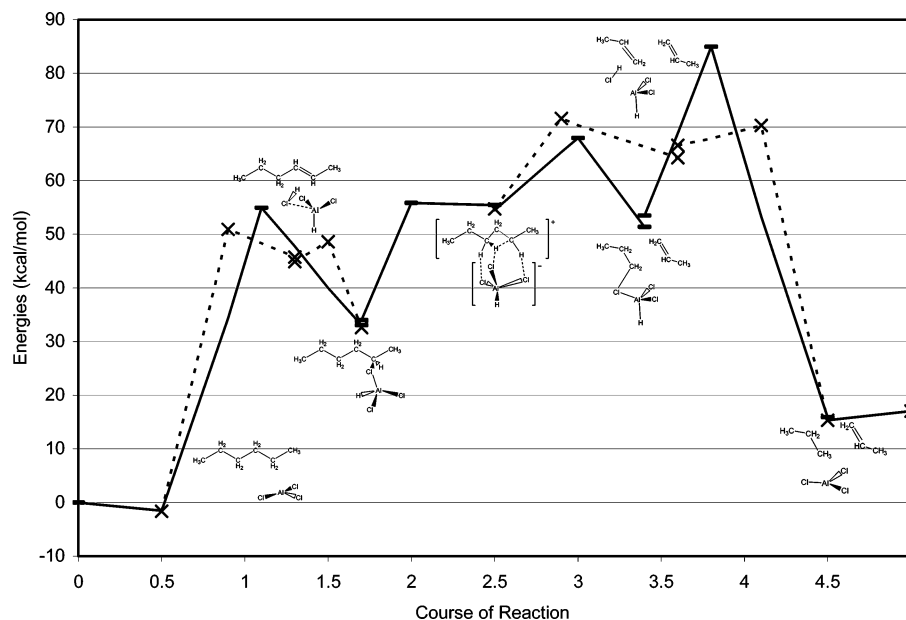


Figure 7. Energy profile for the Lewis acid (AlCl₃) catalytic cycle. Solid lines: main Lewis acid path (bold arrows of Scheme 2). Dashed lines: alternative paths via alkene/Bronsted acid intermediates (double arrows of Scheme 2).

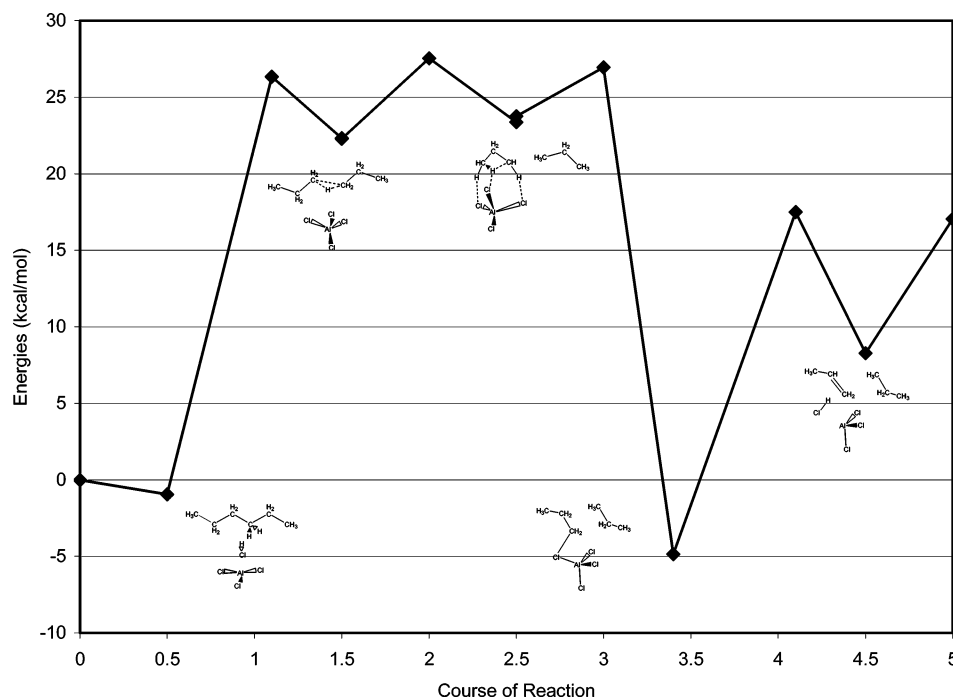


Figure 8. Energy profile for the Bronsted acid ($\text{HCl}\cdot\text{AlCl}_3$) catalytic cycle.

cycle is due to breaking a strong van der Waals bond of the HCl unit to the π bond of the propene molecule.

Minimizations with Al_2Cl_7^- . Here we considered replacing AlCl_3 with the more realistic ionic-liquid Lewis acid Al_2Cl_7^- , searching for the initial $\text{Al}_2\text{Cl}_7^-//\text{C}_6\text{H}_{14}$ complex, the final $\text{Al}_2\text{Cl}_7^-//\text{C}_3\text{H}_8//\text{C}_3\text{H}_6$ complex, and several possible intermediates. Figure 9 presents 3D images of all seven minimized structures.

The five intermediates all feature the catalyst and reactant in very close contact, with a tight anion bridge between an Al and a C atom. In the second and sixth images, the tight connection is a weak hydride bridge, with $R_{\text{AlH}} = 1.9 \text{ \AA}$, $R_{\text{HC}} = 1.14 \text{ \AA}$, and $\theta_{\text{AlHC}} = 134\text{--}159^\circ$, and in the third/fourth/fifth images, the tight connection is a stronger chloride bridge, with $R_{\text{AlCl}} = 2.4 \text{ \AA}$, $R_{\text{ClC}} = 1.9\text{--}2.0 \text{ \AA}$, and $\theta_{\text{AlClC}} = 109\text{--}117^\circ$.

The initial complex is $\text{Al}_2\text{Cl}_7^-//\text{C}_6\text{H}_{14}$ (top image). The hydride transfer apparently cannot occur right away, however, because the initial attraction of an Al atom to an H atom on alkane results in ejection of an AlCl_4^- unit before the hydride is removed. The result is a sandwich-type intermediate, $\text{AlCl}_3//\text{C}_6\text{H}_{14}//\text{AlCl}_4^-$ (second image), but where the hexane is close to the AlCl_3 unit, and the dissociated AlCl_4^- part moves to be physisorbed on the other side of hexane. With the tight AlCl_3 complex now formed, the hydride transfer would likely occur as the next step. Optimization of a chemisorbed complex of $\text{C}_6\text{H}_{13}^+$ resulted in chemisorption to only one of the two catalyst fragments; our example is the $\text{AlHCl}_3^-/\text{C}_6\text{H}_{13}^+//\text{AlCl}_4^-$ complex (third image). We did not try to find an ascended, physisorbed version of this complex. After an assumed β -scission step, our hypothetical scheme would suggest a complex of four fragments (AlHCl_3^- , C_3H_7^+ , C_3H_6 , AlCl_4^-) with a chemisorption of C_3H_7^+ to one of the anions; we optimized two versions of $\text{AlHCl}_3^-/\text{C}_3\text{H}_7^+//\text{C}_3\text{H}_6//\text{AlCl}_4^-$, depending on whether C_3H_7^+ is a primary or secondary carbocation (fourth and fifth images). To produce the propane product and begin regenerating the catalyst, a revolution of the AlHCl_3^- unit was performed, allowing the hydride back-donation from the catalyst to the C_3H_7^+ unit, forming an $\text{AlCl}_3//\text{C}_3\text{H}_8//\text{C}_3\text{H}_6//\text{AlCl}_4^-$ complex (sixth image) with a tight hydride bridge between AlCl_3 and C_3H_8 . Last, we

moved the AlCl_3 unit away from propane and reassembled the Al_2Cl_7^- unit, optimizing a final $\text{Al}_2\text{Cl}_7^-//\text{C}_3\text{H}_8//\text{C}_3\text{H}_6$ complex.

The electronic energies for these seven intermediates are plotted in Figure 10; the x coordinates of these intermediates are listed in Figure 9. The highest energetic intermediate is the complex involving the primary propenium ion; the secondary propenium ion complex is 3 kcal mol^{-1} lower in energy. Activation barriers were not computed (and hence are not shown); they will be left to a followup project which will be aimed more specifically at an ionic liquid mechanism, rather than a general Lewis acid mechanism which was of focus here. We chose to present these exploratory minimizations here because they give evidence that an alkane// AlCl_3 intermediate is likely even with Al_2Cl_7^- as the model catalyst, suggesting that the idealized catalytic cycle presented here should be a useful starting point for computational modeling of the Al_2Cl_7^- ionic liquid mechanism.

Discussion

State of Carbenium Ions. In the Lewis acid cycle (top half of Scheme 3), two of the three carbenium-ion intermediates are stable chemisorbed versions (at 33 and 51 kcal mol^{-1}), each requiring 17 kcal mol^{-1} or more in activation energy to ascend to physisorbed ion-pair or neutral-pair complexes. The physisorbed carbenium-ion intermediate, the protonated dialkylcyclopropane PCP^+ (at 55 kcal mol^{-1}), is the active species that undergoes scission, but is bound by only 1 kcal mol^{-1} . At better levels of theory, this physisorbed ion-pair minimum might possibly disappear for this system. However, in the true ionic liquid, such ion-pair intermediates will be further stabilized, and we would expect PCP^+ to not only be an intermediate but remain as the active species for scission. In fact, physisorbed PCP^+ has been detected on solid AlBr_3 (from Br^- abstraction from 2-bromopropane) by Haw and co-workers.²⁵ This is in contrast to zeolite catalysis, where PCP^+ is apparently not a detectable intermediate,²⁵ but perhaps an accessed “shelf region” on the PES.

On the Differences between Ionic Liquids vs Zeolites. On zeolites, the PCP^+ shelf region appears to be responsible for a

$x=0.5$ $\text{Al}_2\text{Cl}_7^-//\text{C}_6\text{H}_{14}$	 -3943.798745
$x=1$ $\text{AlCl}_3//\text{C}_6\text{H}_{14}//\text{AlCl}_4^-$	 -3943.769188
$x=1.5$ $\text{AlHCl}_3^-//\text{C}_6\text{H}_{13}^+//\text{AlCl}_4^-$	 -3943.721446
$x=2.5$ $\text{AlHCl}_3^-//p\text{-C}_3\text{H}_7^+//\text{C}_3\text{H}_6//\text{AlCl}_4^-$	 -3943.691207
$x=3.5$ $\text{AlHCl}_3^-//s\text{-C}_3\text{H}_7^+//\text{C}_3\text{H}_6//\text{AlCl}_4^-$	 -3943.696725
$x=4$ $\text{AlCl}_3//\text{C}_3\text{H}_8//\text{C}_3\text{H}_6//\text{AlCl}_4^-$	 -3943.743797
$x=4.5$ $\text{C}_3\text{H}_8//\text{C}_3\text{H}_6//\text{Al}_2\text{Cl}_7^-$	 -3943.772274

Figure 9. Images of B3LYP/6-31G(d,p) optimized minima, of relevance to hexane cracking via an Al_2Cl_7^- Lewis acid. Molecular energies in au include ZPVE.

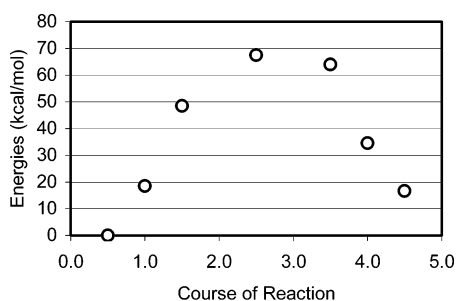


Figure 10. Energy profile for the Al_2Cl_7^- catalytic-cycle minima of Figure 9.

range of isomerization and hydrogen-atom scrambling side reactions. Ionic liquids could offer a good environment to make carbenium ions perform differently than they do in zeolites. First, PCP^+ may be more easily generated because of extra stability in an ionic environment. Second, the liquid phase of ionic liquids makes for constant-contact conditions which may reduce isomerization by speeding up cracking/oligomerization times. Third, the ionic liquid may lead to a wider product distribution than a zeolite which has pore size restrictions. Fourth, the

selection of the cation part of ionic liquids may have an effect on reactivity via concentration or solubility effects.

Bronsted Acid vs Lewis Acid. In their alkane cracking study, Xiao et al.⁹ prepared four different ionic liquids containing 64 mol % AlCl_3 (generating $\text{Al}_2\text{Cl}_6\text{X}^-$ Lewis acid anions), and mixed nonane in each, which generated a wide range of hydrocarbon products. To differentiate between a Bronsted or Lewis mechanism, they tried two variations. When a proton scavenger (EtAlCl_2 or CaH_2) was added, the reaction rate went down; when protons (HCl) were added, the rate went up. Hence, a Lewis acid mechanism apparently does occur, but even the presence of Bronsted-acid impurities is enough to speed up the reaction detectably.

Modeling the mechanisms of these particular catalysts by mimicking them would be foolhardy when no prior knowledge of a Lewis-acid-catalyzed reaction path exists. Therefore, in this work, a simpler Lewis-acid catalyst model was used (AlCl_3) as a first step in understanding a Lewis acid mechanism. Furthermore, the focus here is placed on gaining insight on inherent differences that exist in idealized Bronsted vs Lewis acid catalysis of a particular alkane-cracking reaction when other effects such as full solvation are stripped away. Hence, a similarly sized and similarly neutral Bronsted-acid catalyst model was also used ($\text{HCl}\cdot\text{AlCl}_3$), and we can now compare the Lewis acid and Bronsted acid catalytic cycles presented here for hexane \rightarrow propane + propene.

Quantitatively, the Bronsted acid cycle provided the lower overall reaction barrier (28 vs 83 kcal mol⁻¹), and the lower barrier for the initiation step (26 vs 55 kcal mol⁻¹). This is a manifestation of the rule that the combination of a Lewis acid (AlCl_3) with a Bronsted acid (HCl) usually results in a Bronsted acid that is stronger than either component individually. This is surely the explanation for the enhanced rate Xiao et al. saw when HCl was added to their chloroaluminate ionic liquid.

Qualitatively, there are several mechanistic differences between the Lewis cycle PES with AlCl_3 and the Bronsted cycle PES with $\text{HCl}\cdot\text{AlCl}_3$. In the Lewis acid cycle, physisorbed PCP^+ is the intermediate that leads to cracking (β -scission of hexenium ion), but in the Bronsted acid cycle, it is the intermediate that results from cracking (α -scission of hexanium ion). The initiation steps both result in AlCl_3X^- ions, but in the Lewis cycle it is immediately chemisorbed to $\text{C}_6\text{H}_{13}^+$, while in the Bronsted cycle it is physisorbed to $\text{C}_6\text{H}_{15}^+$. The higher-energy Lewis cycle is prone to producing Bronsted acid catalysts as intermediates. Both cycles prefer to produce a chemisorbed $p\text{-C}_3\text{H}_7^+$ ion that is significantly stabilized and, as Figure 7 shows, would be prone to oligomerizing with approaching alkenes rather than simply ascending to PCP^+ or propene or propane. This might explain the penchant for oligomerization that was also seen in the chloroaluminate ionic liquid.⁹

It is hoped that this comparison will prove useful for future attempts in comparing Bronsted acid mechanisms to Lewis-acid ones.

Summary

Cracking of an all-trans *n*-alkane, via idealized Lewis acid and Bronsted acid catalysis, was examined using B3LYP/6-31G(d,p) calculations. Optimized geometries and transition states were determined for catalyst-reactant complexes, using AlCl_3 and $\text{HCl}\cdot\text{AlCl}_3$ as the Lewis and Bronsted acids. For the Lewis acid cycle, hydride-transfer steps are seen to have large barriers in both forward and reverse directions, and an unstable physisorbed carbenium ion (lying 20 kcal mol⁻¹ above the chemisorbed intermediate) is the launching point for the

β -scission that leads to products. For the Bronsted acid cycle, proton-transfer steps have smaller barriers in both forward and reverse directions, and a semistable physisorbed alkanium ion is the launching point for the alkanium α -scission that leads to products. In the idealized Lewis cycle, formation of HCl units (and hence Bronsted acids) was found to be a common side reaction.

Exploratory optimizations were performed with Al_2Cl_7^- as the catalyst, as motivated by a recent Lewis acid ionic-liquid catalysis of alkane cracking,⁹ and the existence of an $\text{AlCl}_3//\text{C}_6\text{H}_{14}/\text{AlCl}_4^-$ intermediate before hydride abstraction provides evidence that our use of AlCl_3 as a model Lewis acid may be a great starting point for future computational modeling of the ionic liquid mechanisms.

Acknowledgment. This research was funded by NSERC and CFI (Canada). The Laboratory of Computational Discovery (University of Regina) is thanked for computational resources.

Supporting Information Available: Cartesian coordinates of all 22 transition states and the minima of Figure 9. This material is available free of charge via the Internet at <http://pubs.acs.org>.

References and Notes

- (1) Ionic Liquids in Organic Synthesis. *Chem. Eng. News* **2004**, 82 [45], 44.
- (2) Welton, T. *Chem. Rev.* **1999**, 99, 2071.
- (3) Wasserscheid, P.; Keim, W. *Angew. Chem., Int. Ed.* **2000**, 39, 3772.
- (4) Kemperman, G. J.; Roeters, T. A.; Hilberink, P. W. *Eur. J. Org. Chem.* **2003**, 1681.
- (5) Boovanahalli, S. K.; Kim, D. W.; Chi, D. Y. *J. Org. Chem.* **2004**, 69, 3340.
- (6) Qiao, K.; Deng, Y. *J. Mol. Catal. A* **2001**, 171, 81.
- (7) Golezdzinowski, M.; Birss, V. I.; Galuszka, J. *Ind. Eng. Chem. Res.* **1993**, 32, 1795.
- (8) Adams, C. J.; Earle, M. J.; Seddon, K. R. *Green Chem.* **2000**, 2, 21.
- (9) Xiao, L.; Johnson, K. E.; Treble, R. G. *J. Mol. Catal. A* **2004**, 214, 121.
- (10) Olah, G. A.; Halpern, Y.; Shen, J.; Mo, Y. K. *J. Am. Chem. Soc.* **1973**, 95, 4960.
- (11) Zhao, Y.; Bamwenda, G. R.; Wojciechowski, B. W. *J. Catal.* **1993**, 142, 465.
- (12) Glasebrook, A. L.; Phillips, N. E.; Lovell, W. G. *J. Am. Chem. Soc.* **1936**, 58, 1944.
- (13) Corma, A.; Garcia, H. *Chem. Rev.* **2003**, 103, 4307–4365.
- (14) Fokin, A. A.; Schreiner, P. R. *Adv. Synth. Catal.* **2003**, 345, 1035.
- (15) Hunter, K. C.; Seitz, C.; East, A. L. L. *J. Phys. Chem. A* **2003**, 107, 159.
- (16) Becke, A. D. *J. Chem. Phys.* **1993**, 98, 5648.
- (17) Lee, C.; Yang, W.; Parr, R. G. *Phys. Rev. B* **1988**, 37, 785.
- (18) Frisch, M. J.; Trucks, G. W.; Schlegel, H. B.; Scuseria, G. E.; Robb, M. A.; Cheeseman, J. R.; Zakrzewski, V. G.; Montgomery, J. A.; Stratmann, R. E.; Burant, J. C.; Dapprich, S.; Millam, J. M.; Daniels, A. D.; Kudin, K. N.; Strain, M. C.; Farkas, O.; Tomasi, J.; Barone, V.; Cossi, M.; Cammi, R.; Mennucci, B.; Pomelli, C.; Adamo, C.; Clifford, S.; Ochterski, J.; Petersson, G. A.; Ayala, P. Y.; Cui, Q.; Morokuma, K.; Malick, D. K.; Rabuck, A. D.; Raghavachari, K.; Foresman, J. B.; Cioslowski, J.; Ortiz, J. V.; Stefanov, B. B.; Liu, G.; Liashenko, A.; Piskorz, P.; Komaromi, I.; Gomperts, R.; Martin, R. L.; Fox, D. J.; Keith, T.; Al-Laham, M. A.; Peng, C. Y.; Nanayakkara, A.; Gonzalez, C.; Challacombe, M.; Gill, P. M. W.; Johnson, B. G.; Chen, W.; Wong, M. W.; Andres, J. L.; Head-Gordon, M.; Replogle, E. S.; Pople, J. A. *Gaussian 98*, revision A.9; Gaussian, Inc.: Pittsburgh, PA, 1998.
- (19) *PQS 3.0*; Parallel Quantum Solutions; Fayetteville, AR, 2004.
- (20) Baker, J. *J. Comput. Chem.* **1986**, 7, 385.
- (21) Brown, D. E.; Moffatt, D. J.; Wolkow, R. A. *Science* **1998**, 279, 542.
- (22) Wolkow, R. A.; Lopinski, G. P. Private communication.
- (23) Sie, S. T. *Ind. Eng. Chem. Res.* **1992**, 31, 1881.
- (24) Kazansky, V. B. *Catal. Today* **1999**, 51, 419.
- (25) Haw, J. F. *Phys. Chem. Chem. Phys.* **2002**, 4, 5431.